Revealing electronic nature of broad bound exciton bands in two-dimensional semiconducting WS_2 and MoS_2

Jingzhi Shang,[1,2] Chunxiao Cong,[3] Xiaonan Shen,[2] Weihuang Yang,[2] Chenji Zou,[2] Namphung Peimyoo,[2] Bingchen Cao,[2] Mustafa Eginligil,[2,5] Wei Lin,[4] Wei Huang,[1,5,6,*] and Ting Yu[2,†]

[1]*Institute of Flexible Electronics, Northwestern Polytechnical University (NPU), 127 West Youyi Road, Xi'an 710072, China*

[2]*Division of Physics and Applied Physics, School of Physical and Mathematical Sciences, Nanyang Technological University, Singapore 637371*

[3]*State Key Laboratory of ASIC & System, School of Information Science and Technology, Fudan University, Shanghai 200433, China*

[4]*Fujian Provincial Key Laboratory of Semiconductor Materials and Applications, Collaborative Innovation Center for Optoelectronic Semiconductors and Efficient Devices, Department of Physics, Xiamen University, Xiamen 361005, China*

[5]*Key Laboratory of Flexible Electronics (KLOFE) and Institute of Advanced Materials (IAM) National Jiangsu Synergetic Innovation Center for Advanced Materials (SICAM), Nanjing Tech University (NanjingTech), 30 South Puzhu Road, Nanjing 211816, China*

[6]*Key Laboratory for Organic Electronics and Information Displays (KLOEID) and Institute of Advanced Materials (IAM), Nanjing University of Posts and Telecommunications Nanjing 210023, Jiangsu, China*

(Received 31 May 2017; published 13 December 2017)

Owing to unique electronic, excitonic, and valleytronic properties, atomically thin transition metal dichalcogenides are becoming a promising two-dimensional (2D) semiconductor system for diverse electronic and optoelectronic applications. In an ideal 2D semiconductor, efficient carrier transport is very difficult because of lacking free charge carriers. Doping is necessary for electrically driven device applications based on such 2D semiconductors, which requires investigation of electronic structure changes induced by dopants. Therefore probing correlations between localized electronic states and doping is important. Here, we address the electronic nature of broad bound exciton bands and their origins in exfoliated monolayer (1L) WS_2 and MoS_2 through monitoring low-temperature photoluminescence and manipulating electrostatic doping. The dominant bound excitons in 1L WS_2 vary from donor to acceptor bound excitons with the switching from *n*- to *p*-type doping. In 1L MoS_2, two localized emission bands appear which are assigned to neutral and ionized donor bound excitons, respectively. The deep donor and acceptor states play critical roles in the observed bound exciton bands, indicating the presence of strongly localized excitons in such 2D semiconductors.

DOI: 10.1103/PhysRevMaterials.1.074001

I. INTRODUCTION

The emerging transition metal dichalcogenide (TMD) layers as atomically thin semiconductors have attracted great attention and become an exciting material system for fundamental research [1] and device applications [2]. Fascinating properties of such 2D semiconductors have been uncovered such as strong quantum confinement [3,4], robust spin-obit coupling [5,6], enhanced Coulomb interaction [7], large excitonic effect [8], unique valley polarization [9], and distinguished many-body interactions [10]. Recently, monolayer (1L) field-effect transistors [11], photodetectors [12], light-emitting diodes [13], and nanolasers [14] have been demonstrated as counterparts of conventional Si and III-V-based devices, which open up many opportunities for developing the next-generation electronics and optoelectronics with desirable features such as ultrathin thickness, high transparency, and great flexibility. In most used semiconductor devices, efficient carrier transport is necessary. However, the electrical conductivity in a perfect semiconductor is very limited owing to lack of free charge carriers. In practice, doping has become a crucial strategy to bring in sufficient free carriers. Natural and artificial semiconductors contain some impurities and defects more or less, which typically result in unintentional doping. In 1L MoS_2 and WS_2, such doping has also been found [15,16] while the origin is still under discussion. Therefore investigation of unintentional doping mechanisms of these promising 2D semiconductors is important to boost practical device applications.

Theoretically, the formation energies of native defects and their influence on the electronic structure of 1L MoS_2 were investigated based on the density functional theory [17]. Meanwhile, the modifications of optical and electrical conductivities caused by point defects in MoS_2 and WS_2 were simulated according to a large-system tight-binding model [18]. To realize *p*- and *n*-type doping in MoS_2, different substitutive and absorbable dopants were considered such as Nb, Re, and molecular ions [19]. Experimentally, surface morphologies of structural defects in layered MoS_2, $MoSe_2$, WS_2, and WSe_2 were studied by scanning tunneling microscopy (STM) [20,21]. The elements in natural MoS_2 crystals were examined by inductively coupled plasma mass spectrometry (ICPMS), where diverse types and amounts of impurities were observed in different molybdenite sources [22,23]. Although some progress has been made on the structures and types of defects in as-exfoliated 1L WS_2 and MoS_2, their impact on unintentional doping remains unclear. Thus direct experimental explorations are desired to reveal native localized states and their doping dependence. Particularly, the low-temperature photoluminescence (PL) is sensitive to impurity- and defect-induced gap states in traditional semiconductors such as Si [24], GaAs [25], and

*Corresponding author: iamwhuang@njtech.edu.cn
†Corresponding author: yuting@ntu.edu.sg

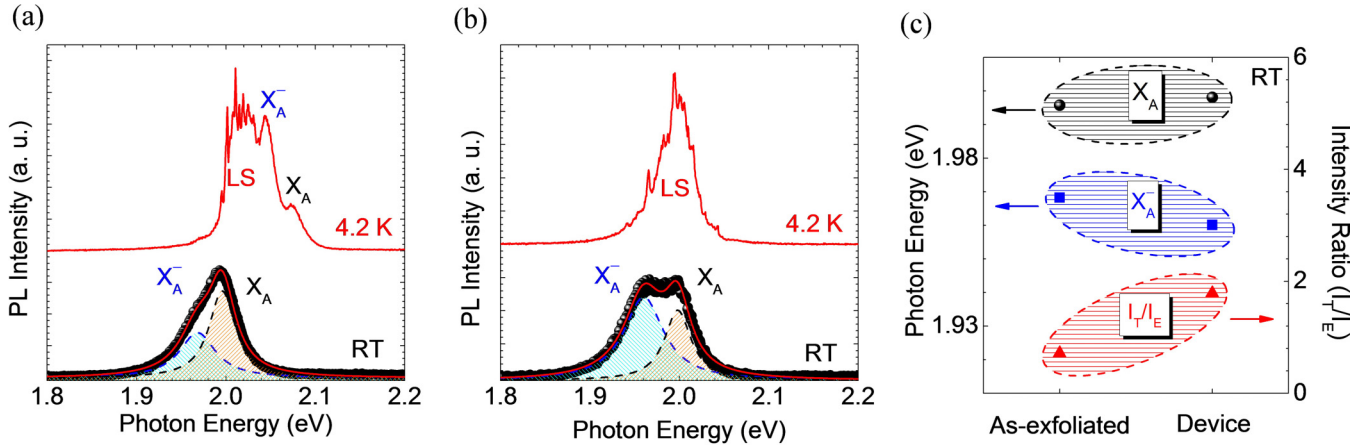

FIG. 1. Photoluminescence of 1L WS_2. (a) Photoluminescence spectra of as-exfoliated 1L WS_2 collected at RT (300 K) and 4.2 K, respectively. (b) Photoluminescence spectra of a field-effect device using exfoliated 1L WS_2 taken at RT and 4.2 K, respectively. (c) Photon energies of X_A, X_A^-, and intensity ratios of I_T/I_E in as-exfoliated 1L WS_2 and the field-effect device at RT. Localized state emission is denoted by LS. I_E and I_T represent integrated intensities of X_A and X_A^-, respectively.

ZnO [26], where optical transitions with lower energies than the ones of the band gaps or excitons have been linked to specific gap states caused by donors, acceptors, vacancies, and so on. Recently, low-energy emission bands were observed in exfoliated 1L MoS_2 [15], $MoSe_2$ [27], WS_2 [28,29], and WSe_2 [13], while less attention was paid to their electronic nature and correlations with different types of impurities and defects.

Here, we have identified dopant-related localized states and studied their origins in exfoliated 1L WS_2 and MoS_2 by low-temperature PL spectroscopy with tunable electrostatic doping. Low-energy PL bands have been observed, which reflect the excitonic transitions involved with localized gap states. The prevailing emission caused by localized states varies with the doping, which provides us hints to identify the types of bound excitons and narrow down the scope of the underlying impurities and defects. Moreover, specific impurity dopants and structural defects responsible for low-energy PL have been proposed and analyzed. As a result, the observed optical transitions associated with localized gap states have been correlated with donor and acceptor-bound excitons.

II. METHODS

The used 1L WS_2 and MoS_2 were mechanically exfoliated from natural MoS_2 and synthesized WS_2 crystals (purchased from 2D semiconductors Inc.) onto SiO_2/Si substrates by the scotch tape technique [30], where the thickness of the top SiO_2 is 280 nm and the underlying Si is p-type doped. The field-effect devices were fabricated by following a standard procedure including e-beam lithography, electrode deposition, and wire-bonding as reported previously [31]. The back-gate voltage (V_g) was applied by a Keithley 4200 characterization system. A customized micro-PL/Raman spectroscopic system was used to carry out PL measurements, where a liquid helium cryostat, a vacuum tube, and a three-dimensional piezostage were included. The sample chamber was initially pumped down to an ultrahigh vacuum (i.e., pressure of $\sim 10^{-5}$ mbar) to minimize the effect of the ambient surroundings (e.g., gas molecules of H_2O and O_2). After that, high-purity (99.9995%) helium gas was flowed into the chamber as a protection and cooling medium to maintain a low pressure of 18 mbar. The samples were excited by a commercial 532-nm Nd:YAG laser and a 50 × objective lens was used to focus the laser beam on the sample surface with a spot size of ~1 μm. A grating (600/mm) spectrometer was employed to measure the PL signals, where a thermoelectrically cooled detector was equipped.

III. RESULTS AND DISCUSSION

The low panel of Fig. 1(a) shows the room-temperature (RT) PL spectrum of the as-exfoliated 1L WS_2, where the emission profile consists of two components due to exciton (X_A) and negative trion (X_A^-) emission components at 1.97 and 2.0 eV, respectively. With the temperature decreasing to 4.2 K, both bands blueshift and narrow as presented in the upper panel of Fig. 1(a). The new emission features, i.e., a broad emission assembly with several narrow spikes around 2.02 eV, appear at the low-energy side, which is attributed to optical transitions associated with localized states within the band gap. The broad localized state band as indicated by LS vanishes at RT mainly due to the increasing thermal disorder and quenching, which is consistent with the typical temperature-dependent behaviors of the bound exciton emission [32]. Besides, the very narrow emission peaks in 1L TMD and BN have recently been studied in details, which are associated with quantum emitters due to defects (e.g., vacancies) and/or nanoclusters [33–37]. Hence, instead of the investigation of each narrow emission spike, we focus on the overall electronic nature of the broad low-energy band as an ensemble of multiple emission components involved with a wide range of localized states. Figure 1(b) presents PL spectra of a field-effect device of 1L WS_2 collected at RT and 4.2 K, respectively. The main emission changes from X_A and X_A^- to localized states with the decrease of temperature. Compared with the PL of the as-exfoliated 1L WS_2 at 4.2 K [Fig. 1(a)], the localized state emission of this device becomes more dominant and its overall profile shifts to low energies around 2.0 eV, which is possibly

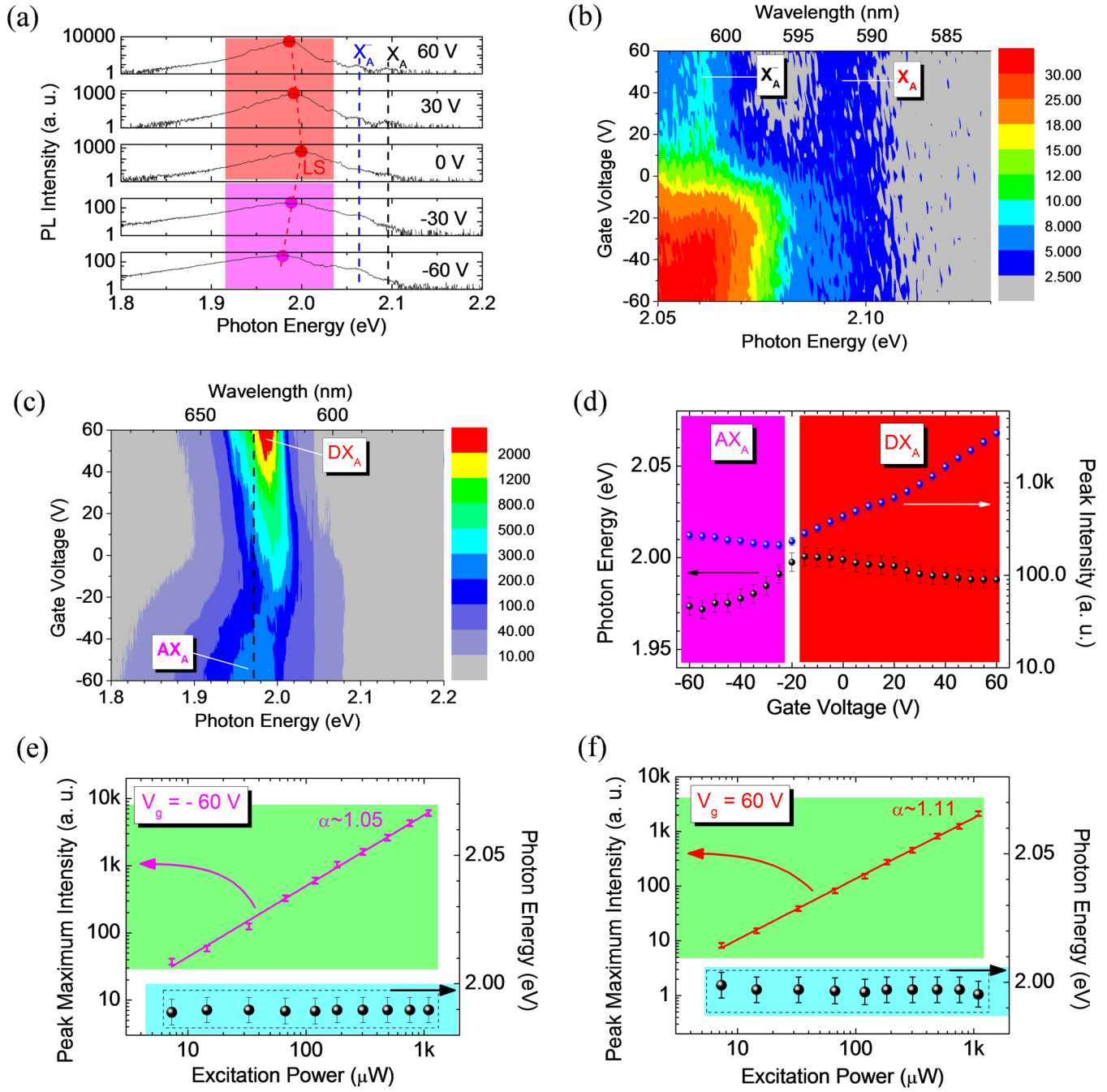

FIG. 2. Photoluminescence of 1L WS_2 under electrical doping and varied photoexcitation. (a) Photoluminescence spectra at various gate voltages of a 1L-WS_2 field-effect device taken at 4.2 K. [(b) and (c)] Gate-voltage dependent photoluminescence maps in the spectral regions of 2.05–2.13 and 1.8–2.2 eV, respectively. (d) Peak maximum position and intensity of LS vs gate voltage. [(e) and (f)] Peak maximum position and intensity of LS vs excitation power at the back-gate voltages of –60 and 60 V, respectively. Solid lines in (e) and (f) are linear fit curves with the slopes (α). The excitation power in (a)–(c) is 67 μW, corresponding to a power density of ~8.5 kW/cm^2.

caused by the different unintentional doping. As indicated by the PL data at RT [Fig. 1(c)], the photon energy of X_A (or X_A^-) in the 1L WS_2 device blueshifts (or redshifts) and the intensity ratio of X_A^- to X_A increases compared with those of the as-exfoliated 1L WS_2, hinting at the relatively high n-type doping in this device. Similar energy shifts and intensity changes have been observed in the electrically gated 1L WS_2 devices with the increasing electron doping [28,29,31], which support the argumentation here. Note that, for exfoliated and transferred 1L WS_2 flakes, the intensity ratio of X_A to X_A^- generally varies from sample to sample and the precise mechanisms can be diverse in reality. For examples, the flake morphology, the contact with the substrate, and the electrical stress may affect the PL properties [38,39]. In addition, at 4.2 K, the components of X_A and X_A^- in Fig. 1(b) can be seen when the PL intensity is plotted in logarithmic scale [see Fig. 2(a)].

Figure 2(a) presents PL spectra of a 1L WS_2 field-effect device collected at different values of V_g, where X_A, X_A^-, and

LS appear as indicated via guidelines. The PL map versus V_g and energy in the range of 2.05–2.13 eV is shown in Fig. 2(b), where X_A and X_A^- components are more distinguishable with the separation of 32 ± 3 meV at $V_g > 0$ V. Here, we focus on the gate-dependent behavior of LS in the corresponding PL map [Fig. 2(c)]. The LS emission shows different dependence above and below –20 V. More clearly, the peak energy and the peak intensity versus V_g have been plotted in Fig. 2(d). With the increase of V_g from –60 to 60 V, the emission energy blueshifts and the peak intensity decreases at $V_g < -20$ V, and vice versa at $V_g > -20$ V. Such changes result from the switching of the dominant bound excitons as discussed later. Figures 2(e) and 2(f) present the excitation power dependence of LS obtained at $V_g = -60$ and 60 V, respectively, where the dependence is nearly linear and the shifts of the emission photon energies (i.e., within the error range) cannot be fully resolved. According to experimental and theoretical studies on excitation-power dependent PL of semiconductors [40–42], the slopes of near-band-edge emission components due to donor and acceptor bound excitons are $\geqslant 1$, which generally depend on the excitation conditions and the sample quality. In particular, the expected slopes of these bound excitons are close to 1 when the nearly resonant excitation laser is used for a relatively high-quality sample [41,42]. The corresponding PL maps and the estimated Fermi levels of this device under various doping conditions have been shown as Figs. S1 and S2 in Ref. [43]. In another 1L WS_2 field-effect device, at the larger V_g range from –120 to 60 V, such doping-induced changes of intensity and position of the LS emission become more obvious (Fig. S3 in Ref. [43]), which also indicates the presence of similar types of localized states although the unintentional doping levels of different 1L WS_2 devices vary.

In the present spectral range, we consider the possible emission species including neutral donor-bound exciton (DX_A), neutral acceptor-bound exciton (AX_A), donor-acceptor pairs (DAP), ionized donor bound exciton (D^+X_A), and ionized acceptor bound exciton (A^-X_A) accounting for the observed LS emission. Firstly, according to theoretical studies [44], D^+X_A or A^-X_A in a semiconductor material typically requires a heavier effective mass of hole or electron, respectively, and thus these two types of bound excitons generally cannot coexist when the effective masses of hole and electron are not equal. In 2D semiconductors, the binding energy of D^+X_A is predicted to be dependent on the critical mass ratio σ_c (i.e., the maximum value for stable D^+X_A) and D^+X_A remains stable until $\sigma_c = 0.88$ [45]. Previous studies of 1L WS_2 have shown an effective mass ratio of electron to hole (σ) of 0.74 [46], 0.84 [47], 0.83 [48] or 0.98 [49], where three of four calculations [46–49] suggest $\sigma_c < 0.88$ and all indicate a heavier effective hole mass in such 1L WS_2. Therefore, in our case, the D^+X_A excitons are preferred rather than the A^-X_A excitons. Secondly, within the rest three species, the emission due to DAP normally shows the sublinear excitation power dependence [41], different from those of DX_A and AX_A excitons. Hence the observed low-energy bands with the nearly linear power dependence are unlikely caused by DAP. Lastly, the roles of DX_A, AX_A, and D^+X_A need to be further analyzed. Normally, the donor-bound or acceptor-bound excitons are more pronounced in *n*- or *p*-type semiconductors, respectively. For example, in most as-grown ZnO (i.e., *n*-type), the emission due to donor-bound excitons is usually dominant in low-temperature PL spectra rather than other localized emission states [50]. At $V_g = 0$ V, this field-effect device of 1L WS_2 is *n*-doped (Fig. S4 in Ref. [43]) and the main impurity dopants are supposed to be donors. Furthermore, the charged carriers (i.e., electrons) bound to donor or acceptor ions would be affected by the electrostatic environment. With the increase in electron doping, the amount of AX_A is expected to decrease due to the increasing probability of the compensation between electrons and the holes bound to acceptor ions; DX_A is more favorable than D^+X_A considering that a DX_A consists of a D^+X_A and an additional electron. For 1L TMDs, experimental studies have shown that the excitons are more pronounced around the charge neutral state and the trions become more important with the increase of doping [27,31,51]. Moreover, we can interpret that a D^+X_A contains an ionized donor and an exciton, and thus the increase of excitons in the charge neutral environment is in favor of the formation of D^+X_A. In other words, D^+X_A prefers to exist in the charge neutral environment rather than the negatively charged surrounding and thus cannot account for the observed intensity changes at $V_g > -20$ V [Fig. 2(c)]. In our case, the LS band presents different dependence of PL peak intensities and energies above and below –20 V, which indicates two kinds of dominant emission species involved here. At $V_g > -20$ V, the LS intensity rapidly increases with the rising electron concentration, which is consistent with the emission features due to DX_A discussed above. Meanwhile, with the electron withdrawing at $V_g < -20$ V, the localized emission at the lower photon energies, showing the opposite features to those of DX_A, is mainly attributed to AX_A. In addition, the AX_A excitons typically own larger binding energies than those of DX_A excitons [52], which is consistent with the observations here. On the whole, our observations support that DX_A and AX_A take responsibilities for the observed features above and below –20 V, respectively.

Figure 3(a) shows the PL map of a field-effect device of exfoliated 1L MoS_2 versus photon energy and V_g, where five components have been observed and marked by X_B, X_A, X_A^-, L_1, and L_2, respectively. The estimated Fermi levels of this device at varied voltages are shown as Fig. S5 in Ref. [43]. As known, the spin-orbit interaction is strong in 1L TMD and thus results in a large energy splitting around the valance band maximum, for example, ~0.15 eV in 1L MoS_2 [6,53]. Till now, the doping effect on such spin-orbit coupling has not caused enough attention. In general, the energy splitting of A and B bands in 1L TMDs reflects the strength of spin-orbital coupling. According to our observations, the energy separation between X_A and X_B shrinks with the increase in electron doping (Fig. S6 in Ref. [43]), which suggests a possible weakening of the spin-orbit interaction with the rise in Fermi level. A similar trend can be found in the absorption studies of 1L MoS_2 under electrical gating [54], which is consistent with our PL data. Besides, for the observed change of the energy separation, other factors such as Coulomb screening, state filling, and electrical heating could not be fully ruled out here, which require further investigation. Two PL spectra are presented in Fig. 3(b), where four and five Lorentz functions are used to reproduce the curves at 30 and –30 V, respectively. Note that, at low temperatures (4–10 K), the dominant

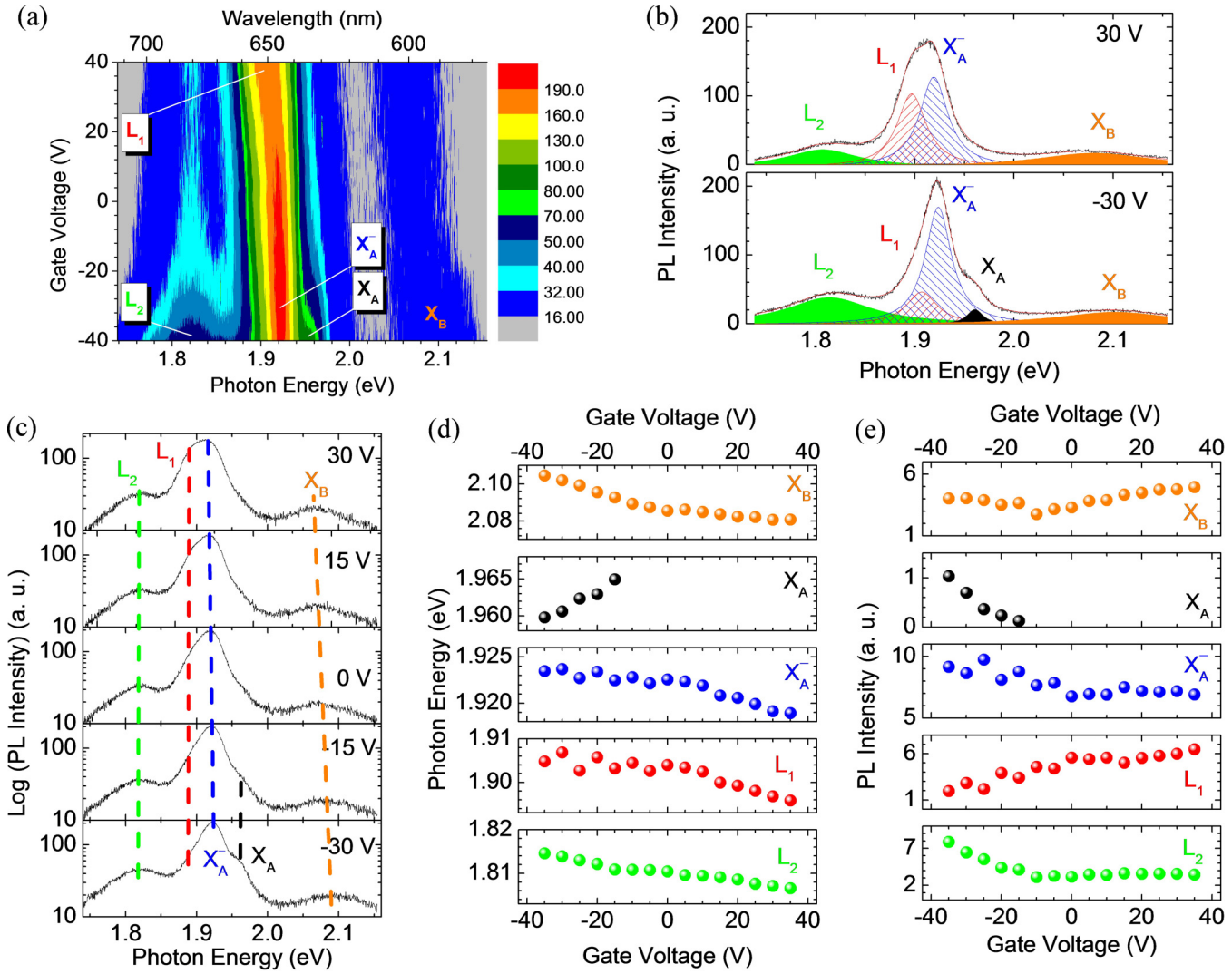

FIG. 3. Photoluminescence of 1L MoS_2 under electrical doping. (a) Photoluminescence map of a field-effect device based on exfoliated 1L MoS_2 at the excitation power of 67 μW and 4.2 K. (b) Photoluminescence spectra taken at –30 and 30 V. (c) Logarithm of photoluminescence intensity vs photon energy taken at various gate voltages. (d) Photon energies of X_B, X_A, X_A^-, L_1, and L_2 vs gate voltage. (f) Integrated intensities of X_B, X_A, X_A^-, L_1, and L_2 vs gate voltage.

emission bands around 1.9 eV of the exfoliated 1L MoS_2 samples have shown different PL widths from 37 to ∼70 meV [53–58], which have been attributed to X_A [53,55,56], X_A^- [54], or the mixture of X_A and X_A^- [54,57], respectively. Beyond these studies [53–58], we have clearly shown that the localized state emission plays an important role in the dominant emission bands around 1.9 eV of typical exfoliated 1L MoS_2 samples with the increase of electron doping at low temperature (Fig. 3). Meanwhile, our observations indicate that, to accurately analyze the low-temperature emission band near the A-exciton transition in a specific exfoliated 1L MoS_2, the possible contributions from X_A, X_A^-, and localized states need to be simultaneously taken into account. Subsequently, the obtained bandwidth of X_A is in the range from 13 to 21 meV (see Fig. S7 in Ref. [43]), which is much smaller than the previously reported ones [53,55,56].

Moreover, the contribution of each component varies with V_g. In particular, L_1 or L_2 plays a more important role in PL at 30 or –30 V, respectively, which implies different doping sensitivities of the corresponding emission species in the *n*-type environment. The spectral evolution can be seen more clearly in Fig. 3(c) where the logarithmic scale is used for the PL intensity. Meanwhile, the enlarged PL spectra around X_A are also plotted in the linear scale (Fig. S8 in Ref. [43]), showing the same tendency. With V_g sweeping from negative to positive values, the contribution of X_A becomes negligible at $V_g > -15$ V. In details, for the doping dependence of photon energies [Fig. 3(d)], only X_A shows a blueshift with the increase of V_g, while the other four components redshift. As shown in Fig. 3(e), the intensities of four components show clear trends with the increase of V_g, where the intensities of X_A, X_A^-, and L_2 decrease while the one of L_1 increases. Besides, the intensity change of X_B is not monotonous, possibly resulting from the competition of different emission species. According to the responses of L_1 and L_2 to the electrostatic doping, the involved bound excitons have been further analyzed with the similar strategy for 1L WS_2 above. On the one hand, considering the enhanced emission and the redshift of L_1 with

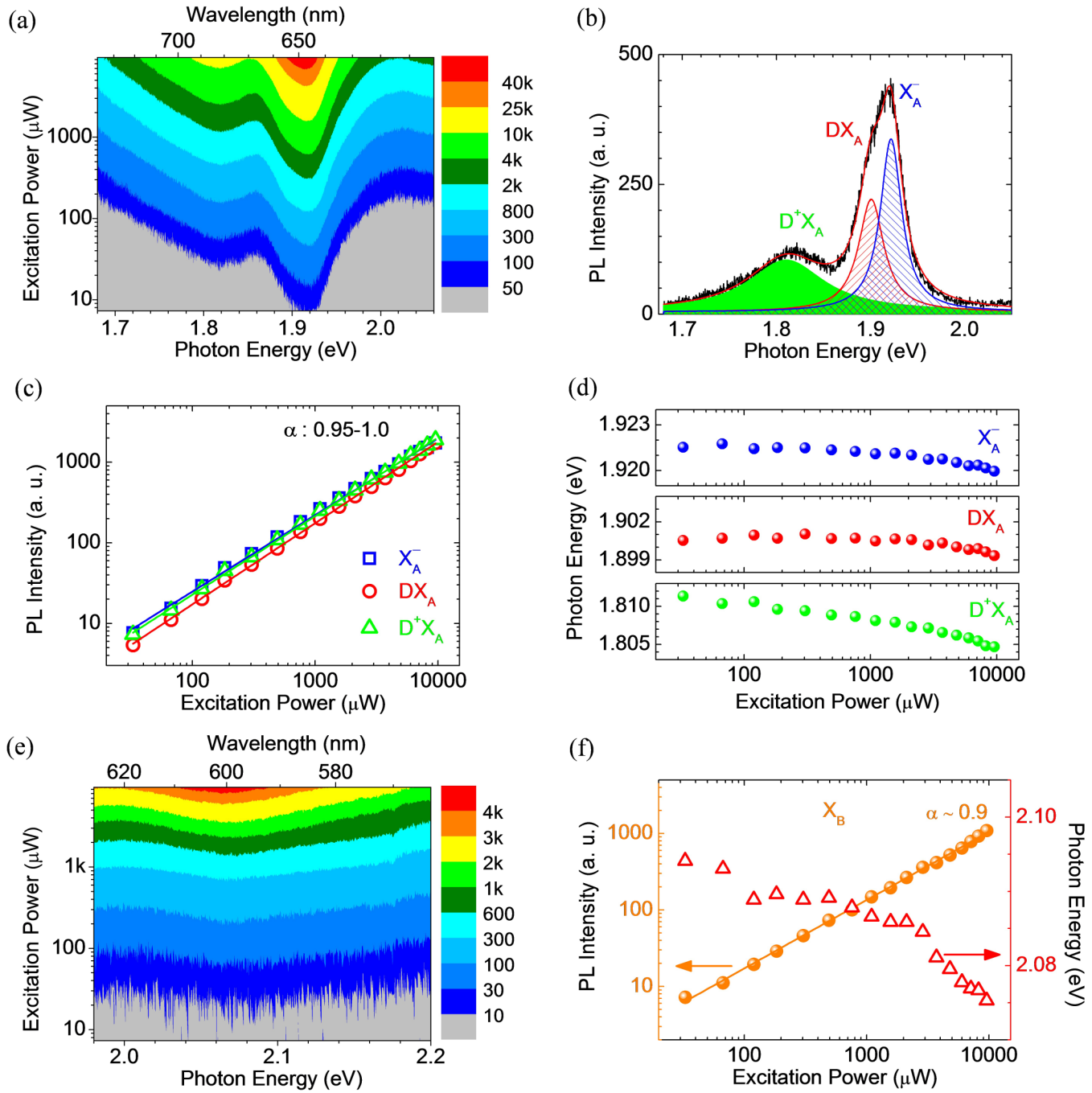

FIG. 4. Excitation dependent photoluminescence of 1L MoS_2. (a) Photoluminescence map of 1L MoS_2 device in the photon energies ranging from 1.68 to 2.06 eV at 4.2 K. (b) Photoluminescence spectrum taken at 67 μW. (c) Excitation-power dependence of integrated intensities of X_A^-, DX_A, and D^+X_A. (d) Excitation-power dependence of photon energies of X_A^-, DX_A, and D^+X_A. (e) Photoluminescence map of 1L MoS_2 device in the photon energies ranging from 1.98 to 2.2 eV. (f) Excitation-power dependence of integrated intensity and photon energy of X_B. The solid lines in (c) and (f) represent the linear fit curves with the slopes (α).

the electron injection, it is attributed to DX_A. On the other hand, the possible roles of DX_A, D^+X_A, and A^-X_A in L_2 need to be further addressed, while DAP unlikely accounts for L_2 seeing that the nearly linear excitation power dependence is presented later [Fig. 4(c)] rather than the typical sublinear behavior of DAP [41]. In details, either D^+X_A or A^-X_A can exist in 1L MoS_2 since different effective mass ratios of electron to hole have been reported such as 0.80 [59], 1.11 [49], 0.92 [47], and 1.76 [10] based on theoretical calculations. Nevertheless, in most *n*-type semiconductors, A^-X_A rarely exists [44,52]. The field-effect device of 1L MoS_2 shows the *n*-type behavior (Fig. S4 in Ref. [43]), and consequently D^+X_A is more prevalent than A^-X_A here. Both AX_A and D^+X_A can result in the observed intensity changes of L_2 [Fig. 3(e)]. The D^+X_A can take responsibility for the observed energy shift of L_2 [Fig. 3(d)], while the expected shift of AX_A is opposite.

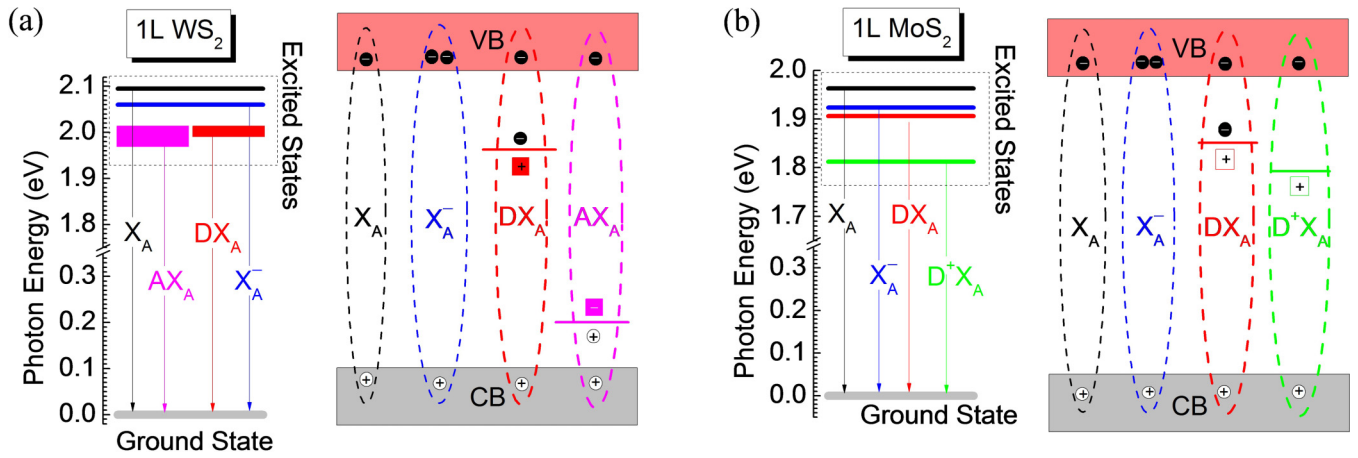

FIG. 5. Excitonic transitions and electronic structures of exfoliated 1L WS_2 and MoS_2. (a) and (b) represent schematics of excitonic transitions with involved charged particles in exfoliated 1L WS_2 and MoS_2, respectively.

The binding energy of DX_A is supposed to be proportional to the ionized energy of donor [60] and the similar dependence has also been found for D^+X_A [50]. In other words, the higher photon energy of DX_A is normally associated with the higher photon energy of D^+X_A [50,61]. Thus similar trends of energy shifts are expected for DX_A and D^+X_A here, which are consistent with our observations for L_1 and L_2. In brief, the L_2 band in 1L MoS_2 is assigned to D^+X_A here.

Figure 4(a) presents the PL intensity map near the A exciton emission *versus* the photon energy and excitation power of a field-effect 1L MoS_2 transistor. The PL spectrum taken at the excitation power of 67 μW can be well reproduced by fitting with three Lorentzian peaks [Fig. 4(b)], which are attributed to X_A^-, DX_A (L_1), and D^+X_A (L_2) according to the discussion above, respectively. The PL intensities of these three bands show the similar linear dependence on the excitation power [Fig. 4(c)]. With the increase in excitation power, the photon energies of three components shift towards lower energies, which is mainly attributed to optically induced electron doping under photoexcitation [Fig. 4(d)] and is consistent with the observations under electrostatic doping [Fig. 3(d)]. Previously, a similar optically induced doping effect has been verified in 1L WS_2 [31]. Furthermore, the PL intensity map around the B exciton emission is presented in Fig. 4(e). With the increase of the excitation power, the photon energy of X_B decreases, while the PL intensity increases in a nearly linear manner [Fig. 4(f)]. At relatively low excitation powers (<1 mW), the shift of X_B is mainly attributed to the rise of Fermi level (via optical doping) associated with the shrinking of spin-orbit splitting, in agreement with the observation [Fig. 3(d)] under electron doping. At high excitation powers (>1 mW), the lattice heating effect caused by photoexcitation may also play a role in the redshift of X_B.

Previously, the low-energy bands around 1.8 eV were observed at low temperatures in many exfoliated 1L MoS_2 samples [9,53,55–57,62,63] and correlated to bound/localized exciton states [53,56,62,63]. Although these emission states have been linked to surface effects [57,63] or defect traps [9], the nature of this low-energy band (i.e., L_2 denoted in our cases) in exfoliated 1L MoS_2 is still not fully understood. On the one hand, the L_2 band can be affected by the dielectric environment such as oxide coverage [63] and substrates [9]. Referring to the typical samples exfoliated on SiO_2/Si substrates, depression or enhancement of L_2 was observed at 10 K for 1L MoS_2 capped by HfO_2 and Al_2O_3 [63] or at 14 K for 1L MoS_2 on the hexagonal BN [9], respectively. For few-layer exfoliated MoS_2, elevation or suppression of L_2 has also been observed with the encapsulation of SiO_2 or Si_xN_y, respectively [15]. Thus the dielectric surrounding indeed impacts the L_2 emission. Two possible reasons, i.e., surface adsorbates [63] and charge transfer [15], were proposed to take responsibilities for the emission changes. Our gated PL measurements have unambiguously demonstrated that the *n*-type electrostatic doping results in the suppression of the L_2 band, supporting the charge transfer mechanism above. On the other hand, impurity elements [22,23] and structural defects [22,64,65] naturally exist in exfoliated MoS_2 samples and consequently the additional gap states can be expected according to theoretical calculations [17–19]. Here, we consider that the observed L_2 band at 4.2 K most probably originates from the unintentional impurity- and defect-induced gap states. Note that, different PL studies of exfoliated 1L MoS_2 on the substrates of SiO_2/Si [53,57,62] and BN [9] have shown the similar peaks to L_2, implying that L_2 most likely originates from the 1L MoS_2 itself rather than the complex of 1L MoS_2 and its surrounding environment. In the freestanding exfoliated 1L MoS_2, the RT PL emission consists of the contributions from both neutral excitons and negative trions [66], showing that as-exfoliated 1L MoS_2 itself is *n*-type even without the substrate-induced doping. Such native *n*-type doping in as-exfoliated 1L MoS_2 is indicative of the presence of impurity and defect related dopants. More evidently, a similar low-energy band was observed at 80 K for a suspended MoS_2 [67], in support of the defective nature rather than the substrate-related mechanism. Experimentally, with α particle irradiation or thermal annealing, the treated 1L MoS_2 showed a new low-energy band with the peak position at ~0.15 eV below the exciton emission at 77–300 K [68], suggesting that the defect sites can result in the low-energy band emission. Note that, compared with the observed L_2 here, the created emission band of the defective sample at 77–300 K [68] shows the different excitation power dependence (i.e.,

sub-linear) and an additional sensitivity to N_2 gas environment, which are probably due to the involved defect structures and impurities by artificial treatments different from those of as-exfoliated ones. Based on the concerns above, L_2 most probably originates from the defective nature of 1L MoS_2 resulting from impurities and structural defects rather than the surface effect caused by the dielectric surroundings, which is also consistent with our assignment of D^+X_A.

Figures 5(a) and 5(b) show the observed excitonic transitions (left panel) and involved electronic levels with charged particles (right panel) in the field-effect devices of 1L WS_2 and MoS_2, respectively. In addition to X_A and X_A^-, the localized emission bands due to DX_A and AX_A are present in 1L WS_2 while DX_A and D^+X_A appear in 1L MoS_2. Empirically, the binding energy of neutral donor/acceptor bound exciton (E_{BE}) linearly depends on the ionization energy (E_i) of the donor/acceptor known as Haynes's rule [60], i.e., $E_{BE} = CE_i$, where C is a constant between 0.09 and 0.23 for 2D and quasi-2D semiconductors [69–71]. In our case, the observed E_{BE} of DX_A is about 0.1 eV in 1L WS_2, which is significantly larger than those of conventional semiconductors [24–26,60]. Hence the neutral donor level in 1L WS_2 should be located within the range from 0.43 to 1.1 eV below the conduction band minimum (CBM). Unlike the dominant emission caused by shallow donor levels in classic semiconductors of Si [60], GaAs [25] and ZnO [26], the deep donor states account for the observed DX_A emission in 1L WS_2. Similarly, the deep acceptor states are responsible for the observed AX_A. Previous theoretical works [72–75] have shown that impurities and structural defects can introduce localized states within the band gap in 1L WS_2 (see Table S1 in Ref. [43]). For example, the substitution impurity of Mn in 1L WS_2 results in deep localized levels [73] close to the observed donor-bound exciton states above. Meanwhile, our simulations show that carbon (C) substitution and single sulphur vacancy in 1L WS_2 also introduce deep energy levels within the electronic band gap, respectively (see Fig. S9 in Ref. [43]). Further quantitative elemental analysis is needed to precisely determine specific impurities and structural defects in 1L WS_2.

In 1L MoS_2, the estimated neutral donor level associated with DX_A is located at 0.26–0.67 eV below CBM by use of the dissociation energy of ~60 meV, i.e., the energy difference between L_1 and X_A extracted from Fig. 3(d). Similarly, the dominant localized state associated with D^+X_A is expected to be deeper than that with DX_A due to the larger dissociation energy of D^+X_A. On the one side, the impurity atoms in natural bulk MoS_2 have been determined by the highly sensitive ICPMS [22,23], where the impurity concentrations depend on the crystal sources [22]. The used natural MoS_2 crystal here is similar to the one of a-MoS_2 in the previous studies [22] and thus analogous impurities can be expected in our 1L MoS_2. Therefore we consider the following dominant impurities of Al, Ca, Cu, Fe, Mg, Mn, P, Na, Ti, W, and Zn (see Table S1 in Ref. [43]). Within these elements, the impurities of Cu, Fe, Mn, and Ti can bring in the localized states nearby the observed donor levels in 1L MoS_2 according to previous theoretical studies [76–79]. Our calculations also indicate that the Fe substitution indeed results in deep localized states (see Fig. S10 in Ref. [43]). On the other side, based on previous [17–19,72,76–80] and our theoretical simulations, we mainly consider the roles of two structural defects, i.e., sulphur vacancy and interfacial Mo, in the localized state emission of 1L MoS_2. For the sulphur vacancy, it can induce two nearby deep states and one shallow level above the valance band maximum (see Fig. S10 in Ref. [43]), which typically act as acceptor levels [17,80] and cannot account for the observed donor bound excitons. In contrast, the interstitial Mo defect in 1L MoS_2 can cause the n-type doping and acts as a donor, where the donor level is 0.25 eV below the CBM [17] and close to our estimated range. Hence, the interstitial Mo defects may be responsibile for the observed transitions of DX_A. Note that, large excitonic effects are significantly underestimated in the most previous theoretical studies [17–19,72–78,80] on electronic band structures of impurity- and defect-modified 1L MoS_2 and WS_2, which will cause the uncertainties to further correlate the chemical structures with localized states, and thus more advanced calculation approaches [10,49] (e.g., GW-BSE) are required for further theoretical verification.

IV. CONCLUSIONS

To sum up, the broad bound exciton bands and their origins in exfoliated 1L WS_2 and MoS_2 have been investigated by low-temperature PL spectroscopy with controllable doping. The dominant emission bands due to localized states are sensitive to the electrical doping, which enable the determination of the correlations of specific bound exciton types with donor and acceptor levels. At 4.2 K, the dominant bound exciton type responsible for the localized emission around 2 eV in 1L WS_2 changes from DX_A to AX_A with the switching from n- to p-type doping, and two localized emission bands around 1.9 and 1.8 eV of 1L MoS_2 are respectively assigned to DX_A and D^+X_A. Particularly, the deep donor and acceptor levels are involved with the observed bound exciton transitions rather than shallow impurity states, highlighting the large bound excitonic effect (i.e., extrinsic) in such 2D semiconductors. Furthermore, possible impurities and structural defects have been analyzed to account for widely observed localized emission bands. This study sheds light on developing the controllable doping strategy for electronic and optoelectronic applications based on 2D semiconductors.

ACKNOWLEDGMENTS

This work is mainly supported by Singapore MOE Tier 1 RG100/15. W.H. thanks the support by the Natural Science Foundation of Jiangsu Province (BM2012010), Priority Academic Program Development of Jiangsu Higher Education Institutions (YX03001), Ministry of Education of China (IRT1148), Synergetic Innovation Center for Organic Electronics and Information Displays (61136003), the National Natural Science Foundation of China (51173081), and Fundamental Studies of Perovskite Solar Cells (2015CB932200). C.C. thanks the support by Natural Science Foundation of Shanghai (16ZR1402500).

[1] X. D. Xu, W. Yao, D. Xiao, and T. F. Heinz, Nat. Phys. **10**, 343 (2014).

[2] Q. H. Wang, K. Kalantar-Zadeh, A. Kis, J. N. Coleman, and M. S. Strano, Nat. Nanotechnol. **7**, 699 (2012).

[3] H. P. Komsa and A. V. Krasheninnikov, Phys. Rev. B **86**, 241201 (2012).

[4] W. Jin, P.-C. Yeh, N. Zaki, D. Zhang, J. T. Sadowski, A. Al-Mahboob, A. M. van der Zande, D. A. Chenet, J. I. Dadap, I. P. Herman, P. Sutter, J. Hone, and R. M. Osgood, Jr., Phys. Rev. Lett. **111**, 106801 (2013).

[5] H. Zeng, G.-B. Liu, J. Dai, Y. Yan, B. Zhu, R. He, L. Xie, S. Xu, X. Chen, W. Yao, and X. Cui, Sci. Rep. **3**, 1608 (2013).

[6] D. Xiao, G. B. Liu, W. X. Feng, X. D. Xu, and W. Yao, Phys. Rev. Lett. **108**, 196802 (2012).

[7] B. Radisavljevic and A. Kis, Nat. Mater. **12**, 815 (2013).

[8] M. M. Ugeda, A. J. Bradley, S.-F. Shi, F. H. da Jornada, Y. Zhang, D. Y. Qiu, W. Ruan, S.-K. Mo, Z. Hussain, Z.-X. Shen, F. Wang, S. G. Louie, and M. F. Crommie, Nat. Mater. **13**, 1091 (2014).

[9] K. F. Mak, K. L. He, J. Shan, and T. F. Heinz, Nat. Nanotechnol. **7**, 494 (2012).

[10] D. Y. Qiu, F. H. da Jornada, and S. G. Louie, Phys. Rev. Lett. **111**, 216805 (2013).

[11] B. Radisavljevic, A. Radenovic, J. Brivio, V. Giacometti, and A. Kis, Nat. Nanotechnol. **6**, 147 (2011).

[12] O. Lopez-Sanchez, D. Lembke, M. Kayci, A. Radenovic, and A. Kis, Nat. Nanotechnol. **8**, 497 (2013).

[13] J. S. Ross, P. Klement, A. M. Jones, N. J. Ghimire, J. Yan, D. G. Mandrus, T. Taniguchi, K. Watanabe, K. Kitamura, W. Yao, D. H. Cobden, and X. Xu, Nat. Nanotechnol. **9**, 268 (2014).

[14] S. Wu, S. Buckley, J. R. Schaibley, L. Feng, J. Yan, D. G. Mandrus, F. Hatami, W. Yao, J. Vuckovic, A. Majumdar, and X. Xu, Nature (London) **520**, 69 (2015).

[15] D. Sercombe, S. Schwarz, O. Del Pozo-Zamudio, F. Liu, B. J. Robinson, E. A. Chekhovich, I. I. Tartakovskii, O. Kolosov, and A. I. Tartakovskii, Sci. Rep. **3**, 3489 (2013).

[16] F. Withers, T. H. Bointon, D. C. Hudson, M. F. Craciun, and S. Russo, Sci. Rep. **4**, 4967 (2014).

[17] J. Y. Noh, H. Kim, and Y. S. Kim, Phys. Rev. B **89**, 205417 (2014).

[18] S. J. Yuan, R. Roldan, M. I. Katsnelson, and F. Guinea, Phys. Rev. B **90**, 041402 (2014).

[19] K. Dolui, I. Rungger, C. Das Pemmaraju, and S. Sanvito, Phys. Rev. B **88**, 075420 (2013).

[20] H. Murata, K. Kataoka, and A. Koma, Surf. Sci. **478**, 131 (2001).

[21] T. W. Matthes, C. Sommerhalter, A. Rettenberger, P. Bruker, J. Boneberg, M. C. Lux-Steiner, and P. Leiderer, Appl. Phys. A **66**, 1007 (1998).

[22] R. Addou, L. Colombo, and R. M. Wallace, Acs. Appl. Mater. Inter. **7**, 11921 (2015).

[23] R. Addou, S. McDonnell, D. Barrera, Z. Guo, A. Azcatl, J. Wang, H. Zhu, C. L. Hinkle, M. Quevedo-Lopez, H. N. Alshareef, L. Colombo, J. W. P. Hsu, and R. M. Wallace, Acs Nano **9**, 9124 (2015).

[24] D. Karaiskaj, M. L. W. Thewalt, T. Ruf, M. Cardona, H.-J. Pohl, G. G. Deviatych, P. G. Sennikov, and H. Riemann, Phys. Rev. Lett. **86**, 6010 (2001).

[25] M. S. Skolnick, C. W. Tu, and T. D. Harris, Phys. Rev. B **33**, 8468 (1986).

[26] D. C. Look, G. C. Farlow, P. Reunchan, S. Limpijumnong, S. B. Zhang, and K. Nordlund, Phys. Rev. Lett. **95**, 225502 (2005).

[27] J. S. Ross, S. Wu, H. Yu, N. J. Ghimire, A. M. Jones, G. Aivazian, J. Yan, D. G. Mandrus, D. Xiao, W. Yao, and X. Xu, Nat. Commun. **4**, 1474 (2013).

[28] G. Plechinger, P. Nagler, J. Kraus, N. Paradiso, C. Strunk, C. Schüller, and T. Korn, Phys. Status Solidi. RRL **9**, 457 (2015).

[29] B. R. Zhu, X. Chen, and X. D. Cui, Sci. Rep. **5**, 9218 (2015).

[30] A.K. Geim, Science **324**, 1530 (2009).

[31] J. Shang, X. Shen, C. Cong, N. Peimyoo, B. Cao, M. Eginligil, and T. Yu, Acs Nano **9**, 647 (2015).

[32] A. Teke, Ü. Özgür, S. Doğan, X. Gu, H. Morkoç, B. Nemeth, J. Nause, and H. O. Everitt, Phys. Rev. B **70**, 195207 (2004).

[33] Y.-M. He, G. Clark, J. R. Schaibley, Y. He, M.-C. Chen, Y.-J. Wei, X. Ding, Q. Zhang, W. Yao, X. Xu, C.-Y. Lu, and J.-W. Pan, Nat. Nanotechnol. **10**, 497 (2015).

[34] M. Koperski, K. Nogajewski, A. Arora, V. Cherkez, P. Mallet, J.-Y. Veuillen, J. Marcus, P. Kossacki, and M. Potemski, Nat. Nanotechnol. **10**, 503 (2015).

[35] A. Srivastava, M. Sidler, A. V. Allain, D. S. Lembke, A. Kis, and A. Imamoğlu, Nat. Nanotechnol. **10**, 491 (2015).

[36] T. T. Tran, K. Bray, M. J. Ford, M. Toth, and I. Aharonovich, Nat. Nanotechnol. **11**, 37 (2016).

[37] J. Wrachtrup, Nat. Nanotechnol. **11**, 7 (2016).

[38] L. Su, Y. Yu, L. Cao, and Y. Zhang, Phys. Rev. Applied **7**, 034009 (2017).

[39] K. Cho, W. Park, J. Park, H. Jeong, J. Jang, T.-Y. Kim, W.-K. Hong, S. Hong, and T. Lee, Acs Nano **7**, 7751 (2013).

[40] D. E. Cooper, J. Bajaj, and P. R. Newman, J. Cryst. Growth **86**, 544 (1988).

[41] T. Schmidt, K. Lischka, and W. Zulehner, Phys. Rev. B **45**, 8989 (1992).

[42] H. Shibata, M. Sakai1, A. Yamada, K. Matsubara, K. Sakurai, H. Tampo, S. Ishizuka, K.-K. Kim, and S. Niki, Jpn. J. Appl. Phys. **44**, 6113 (2005)

[43] See Supplemental Material at http://link.aps.org/supplemental/10.1103/PhysRevMaterials.1.074001 for excitation-dependent PL maps, calculated Fermi levels at varied back-gate voltages, PL data of another device, electrical transport data, photon energy separations at varied back-gate voltages, doping dependence of peak widths, enlarged PL spectra, calculations of electronic band structures, predicted gap states, and excitation power densities.

[44] I. Pelant and J. Valenta, *Luminescence Spectroscopy of Semiconductors* (Oxford Scholarship Online, Oxford, 2012). Chap. 7, pp. 1–90.

[45] L. Stauffer and B. Stebe, Phys. Rev. B **39**, 5345 (1989).

[46] Z. H. Jin, X. D. Li, J. T. Mullen, and K. W. Kim, Phys. Rev. B **90**, 045422 (2014).

[47] H. L. Shi, H. Pan, Y. W. Zhang, and B. I. Yakobson, Phys. Rev. B **87**, 155304 (2013).

[48] T. Scrace, Y. Tsai, B. Barman, L. Schweidenback, A. Petrou, G. Kioseoglou, I. Ozfidan, M. Korkusinski, and P. Hawrylak, Nat. Nanotechnol. **10**, 603 (2015).

[49] A. Ramasubramaniam, Phys. Rev. B **86**, 115409 (2012).

[50] B. K. Meyer, J. Sann, S. Lautenschlager, M. R. Wagner, and A. Hoffmann, Phys. Rev. B **76**, 184120 (2007).

[51] A. M. Jones, H. Yu, N. J. Ghimire, S. Wu, G. Aivazian, J. S. Ross, B. Zhao, J. Yan, D. G. Mandrus, D. Xiao, W. Yao, and X. Xu, Nat. Nanotechnol. **8**, 634 (2013).
[52] B. K. Meyer, *Zinc Oxide* (Springer-Verlag Berlin, Heidelberg, 2010), Vol. 120, p. 169–199.
[53] G. Sallen, L. Bouet, X. Marie, G. Wang, C. R. Zhu, W. P. Han, Y. Lu, P. H. Tan, T. Amand, B. L. Liu, and B. Urbaszek, Phys. Rev. B **86**, 081301 (2012).
[54] K. F. Mak, K. He, C. Lee, G. H. Lee, J. Hone, T. F. Heinz, and J. Shan, Nat. Mater. **12**, 207 (2013).
[55] G. Plechinger, J. Mann, E. Preciado, D. Barroso, A. Nguyen, J. Eroms, C. Schuller, L. Bartels, and T. Korn, Semicond. Sci. Technol. **29**, 064008 (2014).
[56] D. Lagarde, L. Bouet, X. Marie, C. R. Zhu, B. L. Liu, T. Amand, P. H. Tan, and B. Urbaszek, Phys. Rev. Lett. **112**, 047401 (2014).
[57] T. Kummell, W. Quitsch, S. Matthis, T. Litwin, and G. Bacher, Phys. Rev. B **91**, 125305 (2015).
[58] M. M. Glazov, T. Amand, X. Marie, D. Lagarde, L. Bouet, and B. Urbaszek, Phys. Rev. B **89**, 201302 (2014).
[59] T. Cheiwchanchamnangij and W. R. L. Lambrecht, Phys. Rev. B **85**, 205302 (2012).
[60] J. R. Haynes, Phys. Rev. Lett. **17**, 860 (1966).
[61] B. K. Meyer, J. Sann, S. Eisermann, S. Lautenschlaeger, M. R. Wagner, M. Kaiser, G. Callsen, J. S. Reparaz, and A. Hoffmann, Phys. Rev. B **82**, 115207 (2010).
[62] T. Korn, S. Heydrich, M. Hirmer, J. Schmutzler, and C. Schuller, Appl. Phys. Lett. **99**, 102109 (2011).
[63] G. Plechinger, F.-X. Schrettenbrunner, J. Eroms, D. Weiss, C. Schüller, and T. Korn, Phys. Status Solidi (RRL) **6**, 126 (2012).
[64] H. Qiu, T. Xu, Z. Wang, W. Ren, H. Nan, Z. Ni, Q. Chen, S. Yuan, F. Miao, F. Song, G. Long, Y. Shi, L. Sun, J. Wang, and X. Wang, Nat. Commun. **4**, 2642 (2013).
[65] J. Hong, Z. Hu, M. Probert, K. Li, D. Lv, X. Yang, L. Gu, N. Mao, Q. Feng, L. Xie, J. Zhang, D. Wu, Z. Zhang, C. Jin, W. Ji, X. Zhang, J. Yuan, and Z. Zhang, Nat. Commun. **6**, 6293 (2015).
[66] N. Scheuschner, O. Ochedowski, A.-M. Kaulitz, R. Gillen, M. Schleberger, and J. Maultzsch, Phys. Rev. B **89**, 125406 (2014).
[67] R. Kumar, I. Verzhbitskiy, and G. Eda, IEEE J. Quantum Electron. **51**, 0600206 (2015).
[68] S. Tongay, J. Suh, C. Ataca, W. Fan, A. Luce, J. S. Kang, J. Liu, C. Ko, R. Raghunathanan, J. Zhou, F. Ogletree, J. Li, J. C. Grossman, and J. Wu, Sci. Rep. **3**, 2657 (2013).
[69] D. A. Kleinman, Phys. Rev. B **28**, 871 (1983).
[70] J. J. Liu and X. J. Kong, Phys. Rev. B **55**, 1349 (1997).
[71] J. J. Liu, Y. X. Li, X. J. Kong, and S. S. Li, Chin. Phys. Lett. **16**, 526 (1999).
[72] A. Carvalho and A. H. Castro Neto, Phys. Rev. B **89**, 081406(R) (2014).
[73] X. Zhao, X. Q. Dai, C. X. Xia, T. X. Wang, and Y. T. Peng, Solid State Commun. **215**, 1 (2015).
[74] Y. Ma, Y. Dai, M. Guo, C. Niu, J. Lu, and B. Huang, Phys. Chem. Chem. Phys. **13**, 15546 (2011).
[75] X. Zhao, X. Dai, and C. Xia, Solid State Commun. **217**, 66 (2015).
[76] S. C. Lu and J. P. Leburton, Nanoscale Res. Lett. **9**, 676 (2014).
[77] Y. C. Cheng, Z. Y. Zhu, W. B. Mi, Z. B. Guo, and U. Schwingenschlogl, Phys. Rev. B **87**, 100401 (2013).
[78] Y. Wang, B. Wang, R. Huang, B. Gao, F. Kong, and Q. Zhang, Physica E **63**, 276 (2014).
[79] X. D. Li, Y. M. Fang, S. Q. Wu, and Z. Z. Zhu, Aip. Adv. **5**, 057143 (2015).
[80] H. P. Komsa and A. V. Krasheninnikov, Phys. Rev. B **91**, 125304 (2015).